Growth, structure and magnetic properties of Co ultrathin films on Cu(111) by pulsed laser deposition

2000 J. Phys.: Condens. Matter 12 783

(http://iopscience.iop.org/0953-8984/12/6/303)

J. Phys.: Condens. Matter **12** (2000) 783–794. Printed in the UK PII: S0953-8984(00)06290-1

Growth, structure and magnetic properties of Co ultrathin films on Cu(111) by pulsed laser deposition

M Zheng†, J Shen‡, J Barthel, P Ohresser§, Ch V Mohan‖ and J Kirschner
Max-Planck-Institut für Mikrostrukturphysik, Weinberg 2, 06120 Halle/Saale, Germany
E-mail: joba@mpi-halle.de (J Barthel)

Received 22 July 1999, in final form 9 November 1999

Abstract. Deposition of Co on Cu(111) substrate by laser ablation changes the morphology, structure and magnetic properties of Co ultrathin films. The pulsed laser deposition method induces a good layer-by-layer growth of Co films and delays the face centred cubic to hexagonal close packed structural phase transition in the films. As a result, the pulsed laser deposited films retain an in-plane easy axis of magnetization at all thicknesses investigated (0–15 monolayers Co) while the thermally deposited films also exhibit a hysteresis loop in the perpendicular direction as soon as the hexagonal close packed structure is dominant in the film. In addition, the suppression of hexagonal close packed stacking in the pulsed laser deposited films leads to a complete antiferromagnetic coupling in Co/Cu/Co/Cu(111) trilayers for both in-plane and out-of-plane magnetization directions.

1. Introduction

In recent years growth and magnetism of face centred cubic (fcc) Fe as well as of fcc Co on both Cu(100) and Cu(111) surfaces have been a matter for detailed investigations. For all cases, the high-temperature fcc phases can be epitaxially stabilized at room temperature or below. The particular importance of epitaxial Co structures has been highlighted since the discovery of giant magnetoresistance in Co/Cu multilayers or superlattices [1]. For technical reasons most current applications of magnetic thin films, e.g. sensors for disk drives and magnetic random access memory, involve the deposition of fcc films with (111) texture. Unfortunately, it is extremely difficult to obtain good layer-by-layer growth in these films because they are susceptible to the incorporation of stacking faults which form at the cost of very little energy. Such structural defects appear to have a strong influence on the magnetic coupling. For example, while polycrystalline sputtered Co/Cu(111) multilayers show antiferromagnetic (AF) coupling and oscillatory magnetoresistance [1], Co/Cu(111) crystalline superlattices grown by molecular-beam epitaxy (MBE) were observed to have either no AF coupling [2] or weak, incomplete AF coupling [3–5]. This was suggested to be due to the growth mode of Co on Cu(111) by MBE as the Co films on a Cu(111) substrate form double-layer islands [6]

† Corresponding author. Present address: Center for Materials Research and Analysis, Department of Physics and Astronomy, University of Nebraska, Lincoln, NE 68588, USA.
‡ Present address: Oak Ridge National Laboratory, PO box 2008, Oak Ridge, TN 37831-6057, USA.
§ Present address: European Synchrotron Radiation Facility, BP 220, F-38043 Grenoble Cedex, France.
‖ Present address: Department of Physics and Astronomy, Louisiana State University, Baton Rouge, LA 70803-4001, USA.

0953-8984/00/060783+12$30.00

or even trilayer islands with one subsurface layer [7]. Further growth of the Cu spacer layer yields twinning structures and they serve as 'magnetic bridges' responsible for partial magnetic coupling of adjacent Co layers [8, 9].

The structure of Co on Cu(111) is also more complicated as it is not immediately obvious which phase of cobalt (fcc or hcp) should develop in the expitaxial films. Now it is generally agreed that the early stages of Co on Cu are dominated by fcc cobalt for the first two monolayers (ML) with only a small fraction of stacking faults. As the film coverage increases beyond 2 ML, hcp stacking faults are introduced and the film gradually transforms into hcp stacking, 5 ML Co almost being fully hexagonal close packed [10, 11]. It is interesting to note that on the Cu(110) surface it is possible to grow fcc Co at least up to thicknesses of 15 ML by MBE using O_2 and H as surfactants [12].

To improve the growth of Co layers on Cu(111), Camarero *et al* used Pb as a surfactant and succeeded in obtaining a highly improved structural quality of Co/Cu(111) superlattices and complete AF coupling [8, 9, 13]. However, a possible disadvantage of this method is that it is difficult to get rid of the floating Pb layer, leaving the question of whether the intrinsic magnetism of the system might be affected by the presence of the Pb overlayer†. On the other hand, the pulsed laser deposition (PLD) technique has been recently demonstrated to be a powerful method to assist two-dimensional growth of ultrathin Fe, Co films on (100) and (111) oriented single crystal Cu substrates [14, 15]. The resulting thin films have very good structure and physical properties. We have reported that layer-by-layer growth of Co layers on Cu(111) substrate and significantly less stacking faults can be achieved by using the PLD method [15]. Here we extend our study on detailed growth and magnetic properties of Co/Cu(111) ultrathin films. We will show that the layer-by-layer growth of the PLD Co/Cu(111) film lasts up to 8 ML and the fcc→hcp transition is delayed until about 6 ML. Scanning tunnelling microscopy and its spectroscopy as well as CO absorption are employed to determine the growth mode of the Co film. Together with the improved growth and structure, the PLD Co/Cu(111) films also display different magnetic properties. Complete AF coupling can be achieved in PLD Co/Cu/Co/Cu(111) trilayers.

2. Experimental aspects

The experiments were carried out in a multichamber ultrahigh vacuum (UHV) system with a base pressure of 5×10^{-11} mbar. This multichamber system includes one large size deposition chamber for PLD equipped additionally with Knudsen type effusion cells; a chamber for preparation and analysis equipped with an electron beam evaporator, with Auger electron spectroscopy (AES) and low energy electron diffraction (LEED); a chamber for scanning tunnelling microscopy (STM) and a chamber for magneto-optical Kerr effect (MOKE) measurement. Prior to the evaporation, the Cu(111) single crystal substrate (Mateck) was cleaned by cycles of Ar^+ sputtering and annealed at 750 K until clean Auger spectra and sharp LEED spots were obtained. The substrate was then kept at 230 K and placed 100 mm away from a Co target (Goodfellow, 4 N purity) for PLD. The output of an excimer laser with KrF (248 nm wavelength, 34 ns pulse length, typical pulse energy 270–300 mJ, and repetition rate 5 Hz) was focused onto the Co target to deposit Co onto the Cu(111) substrate. After deposition the sample was transferred under UHV from the MBE chamber to the STM chamber for topographic characterization and scanning tunnelling spectroscopy (STS) at room temperature. Then the sample was moved to the analysis chamber for LEED observations, intensity–energy LEED (IV-LEED) and AES measurements. For the magnetic characterization

† On Cu(110) by the growth method of [12] no oxygen was found at the surface after atomic hydrogen treatment.

MOKE measurements at different temperatures have been carried out prior to chemical and structural investigations.

For comparison, films on the same Cu(111) single crystal at the same substrate temperature (230 K) were prepared by evaporation from a Co wire (Alfa, 5 N purity) heated by e-beam bombardment; this preparation method in the following we denote as thermal deposition (TD) emphasizing the thermal energy of the evaporated species as well as their moderate deposition rate in contrast to PLD.

PLD and TD are carried out in different units of our UHV system. During evaporation each chamber is kept at a total pressure lower than 2×10^{-10} mbar, the residual gas primarily consisting of H_2. The partial pressure of O_2 and CO(+N_2) remains in the lower 10^{-11} mbar range. Thus at a typical average growth rate of 0.2 ML min^{-1} our samples are exposed to about 0.04 Langmuir ML^{-1} of H_2 and less than 0.01 Langmuir ML^{-1} of O_2 and CO.

As a reference, we evaporated *iron* onto Cu(111) from a standard Knudsen cell located in the PLD chamber yielding layer morphology and structure *identical* to Fe grown by the same TD method in the neighbouring e-beam evaporation chamber [16]. This chamber-independent result together with the striking similarity between the growth modes of Fe and Co on Cu(111) serves as an indication that there is no significant influence of O_2 and CO on our measurements.

3. Results

We observed remarkable differences in the growth morphology between the thermal and the pulsed laser deposited Co films. Figure 1 shows a side-by-side comparison of the morphology of submonolayer (0.3 ML) and higher coverage (2.8 ML, 7.9 ML and 15 ML) Co/Cu(111) films prepared by TD (left column) and PLD (right column). Line scans across parts of the visible film areas are displayed as insets. The TD films exhibit typical multilayer growth: the line profile of a 0.3 ML TD film, e.g. shows that the height of the bigger island is mainly 2 ML with an additional 1 ML high spot on top. The substrate is still not completely wetted even at 2.8 ML and there are four layers exposed on the surface as seen by the line scan through the island.

For the PLD films, on the other hand, the morphology is close to layer-by-layer growth. The line scan through the islands of the 0.3 ML film indicates that the islands are one monolayer high. At 2.8 ML, the third layer is nearly filled while the fourth layer islands just nucleate. The layer filling at each nominal film thickness t can be calculated directly from the histogram of the STM morphology. Figure 2 shows the layer filling as a function of total coverage for the PLD films where the graph clearly serves as proof for their 2D growth mode. Up to 7 ML nominal film thickness there is predominantly only one layer growing at each instant in time. Even in the 7.9 ML PLD film—cf image of figure 1(g)—the seventh monolayer level is filled already to about 95% of its total layer area while the eighth, ninth and tenth level occupy 68%, 24% and 2% respectively of their possible total layer area. We have observed that the PLD films still exhibit a smoother surface even at 15 ML compared to TD films.

It is well known that a major role in the formation of the growth morphology is played by surface diffusion. In our case, at submonolayer coverage, some of the islands in TD films show narrow brims we assume to be diffused Cu from the substrate. From the topographic images shown in figure 1, it is not immediately clear what the chemical identity of the islands is. In order to learn more about the initial growth stage of Co films by TD and PLD, we performed STS measurements. The spectroscopic mode of STM, where the tunnelling current I is recorded as

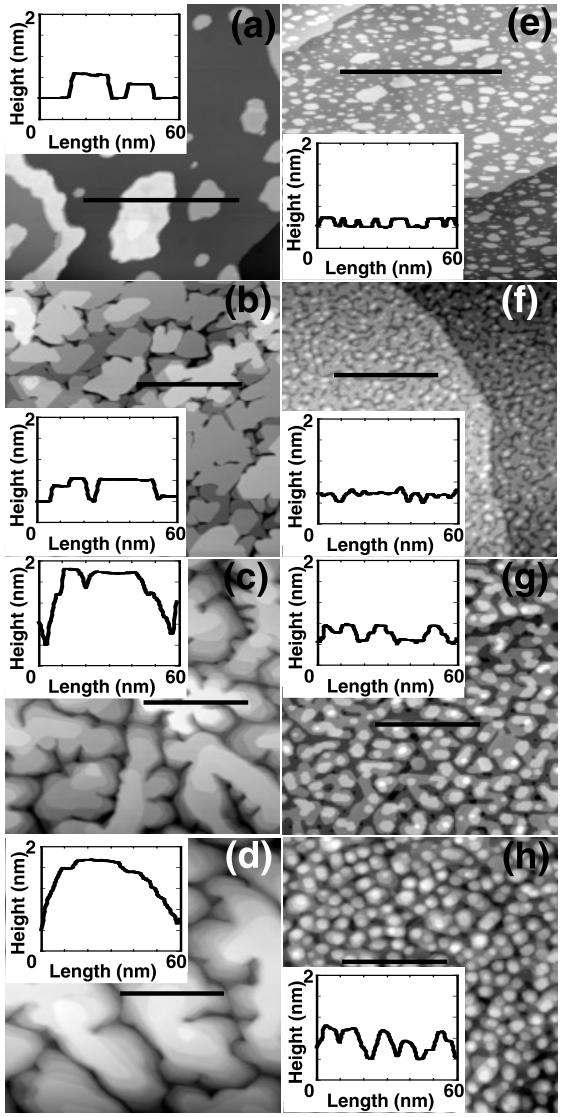

Figure 1. STM topography images of Co/Cu(111) films prepared by thermal deposition—left panel (a)–(d)—and pulsed laser deposition—right panel (e)–(h). The height scale as well as the length of the marked scan line is displayed in the insets. The scale bar length for all figures is 60 nm. The pulsed laser deposited films show layer-by-layer growth while thermal deposition results in 3D growth, forming islands of double layer height already at a net coverage of 0.3 ML. (a) and (e) $t_{Co} = 0.3$ ML, (b) and (f) $t_{Co} = 2.8$ ML, (c) and (g) $t_{Co} = 7.9$ ML, (d) and (h) $t_{Co} = 15$ ML.

a function of the applied bias V with the STM feedback set on hold, yields information on the local electronic structure of the surface. In some cases, it allows us to distinguish between areas consisting of inequivalent atoms [17]. Figure 3 shows current imaging tunnelling spectroscopy (CITS) pictures of both TD and PLD Co/Cu(111) films with 0.3 ML net thickness each at 0.5 V bias voltage together with their corresponding STM topography images (figures 3(a) and (b)).

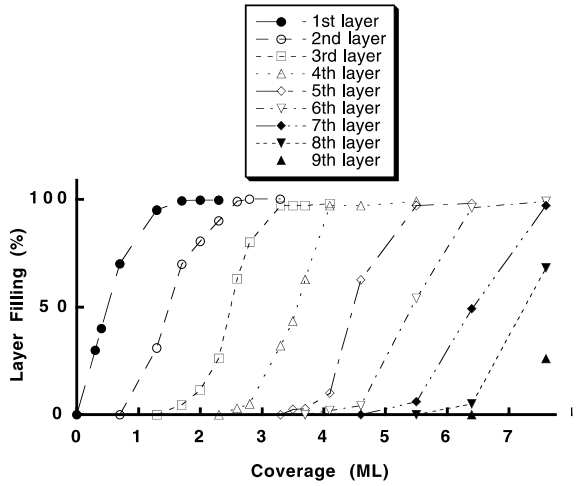

Figure 2. Layer filling as a function of the net coverage t for the PLD Co/Cu(111) films.

Below the CITS pictures, $\mathrm{d}I/\mathrm{d}V$ curves taken from the marked areas as a function of applied bias voltage are shown. In figure 3(c)—the CITS picture of the TD film—the contrast between the islands and the substrate is clearly distinguishable. A one layer deep substrate hole in the middle of the image marked '2' and the brim† around the large island at the left edge marked '3' display the same grey level as the substrate ('1') indicating they are of the same Cu origin. This finding is further backed by the respective STS curves shown in figure 3(e). Apparently the curves taken from the brim, the hole and the substrate are virtually the same, which means they are from the same origin, namely a Cu state, but the curve obtained on top of the island appearing in bright contrast (marked '4') is quite different from that, which means it originates most probably from a Co state.

For PLD films, neither the STS image nor the $\mathrm{d}I/\mathrm{d}V$ curves exhibit contrast between the islands and the substrate. This implies that in the PLD case either Co atoms are incorporated into the substrate surface layer, squeezing out Cu atoms which in turn diffuse onto the top of incorporated Co (note the islands are always only one layer high!) or Co and Cu interdiffuse to form Co–Cu alloys resulting in uniformly mixed states. The dark contour lines of the islands and steps in the STS image of figure 3(d) most probably arise from the lack of the responsible surface state at step edges.

To determine whether the PLD films form a Co–Cu alloy in the initial stage of growth, we performed a CO 'titration' experiment similar to that used in [6]. It has been demonstrated that the main desorption peak appears at a temperature of 170 K for CO on Cu(111) [18] and 430 K for CO on Co(0001) [19]. Thus, in the Co/Cu(111) system, at room temperature CO can just be left adsorbed on pure Co areas [18, 19]. In addition, CO adsorption on Co(0001) appears as $(\sqrt{3} \times \sqrt{3})\mathrm{R}30^\circ$–CO reconstruction and the overall morphology of the Co islands remains unchanged by CO adsorption [7]. Following [7], we exposed both PLD and TD films to about 3000 Langmuir of CO immediately after deposition at 230 K, i.e. still during the process of warming up to room temperature. Subsequently

† It is difficult to reproduce the narrow brims on a halftone print. In figure 3(a) a contrast enhanced portion of the topography image displaying the brim around one particular island is inserted. Similar features are found around almost all islands of submonolayer TD Co/Cu(111) films.

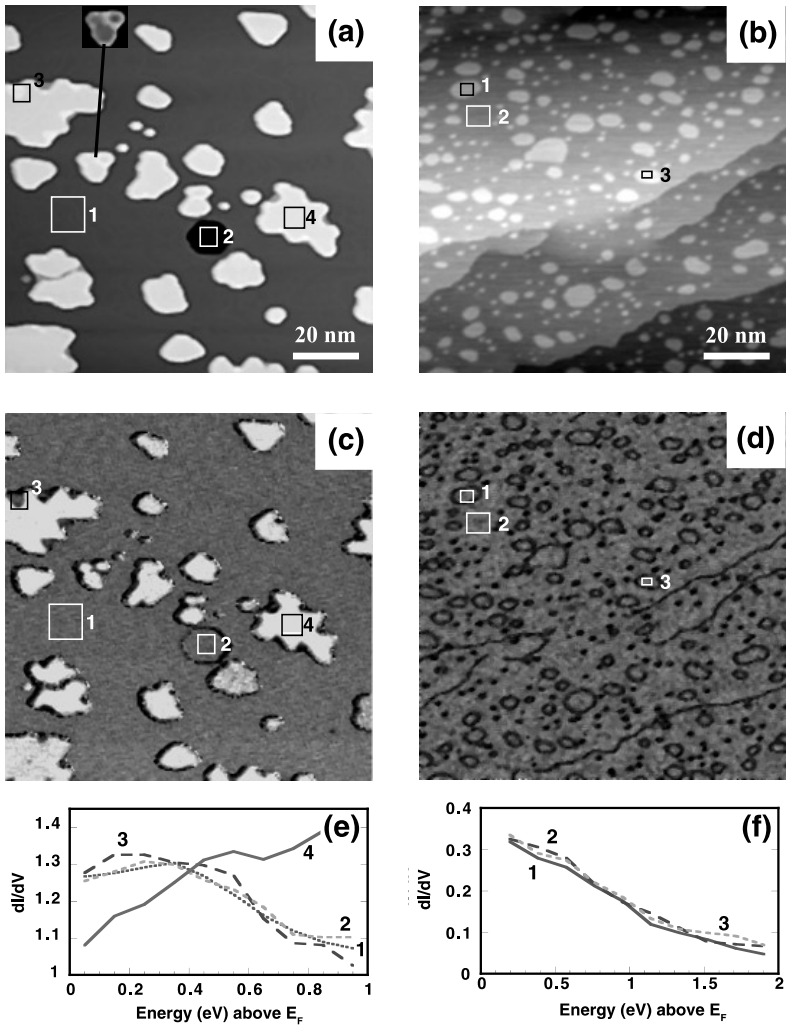

Figure 3. (a) and (b)—STM topography images of 0.3 ML net coverage Co/Cu(111) films. The inset in 3(a) displays a contrast-enhanced island. The corresponding STS images (c) and (d) display for each pixel the total tunnelling current at a preselected voltage measured with the STM feedback switched off. The tunnelling bias voltage is 0.5 eV. (a), (c) TD film; (b), (d) PLD film. (e) $\mathrm{d}I/\mathrm{d}V$ as a function of applied bias for the marked regions shown in (c) = TD film: 1—at the Cu surface, 2—inside a hole of the surface layer, 3—boundary region of a two layer high island, 4—central region of another two layer high island; (f) $\mathrm{d}I/\mathrm{d}V$ curves for the PLD film (d): 1,3—top of a one layer high island, 2—at the bare Cu surface.

the atomically resolved STM imaging of the CO reconstruction pattern was done at room temperature.

Figure 4 shows the image of 0.7 ML TD-Co films after CO adsorption. The central bilayer island is covered by a wide $(\sqrt{3} \times \sqrt{3})\mathrm{R}30^{\circ}$–CO reconstruction which indicates that at least the top layer of the central island must be Co while there is no indication of such structure

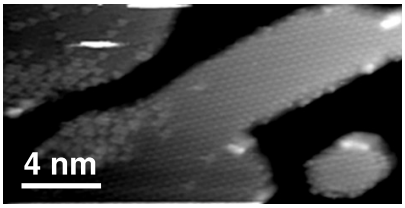

Figure 4. STM image of a 0.7 ML Co film TD grown at 230 K after exposure to 3000 L of CO. CO has been absorbed by Co and forms a $(\sqrt{3} \times \sqrt{3})R30^\circ$ reconstruction superstructure.

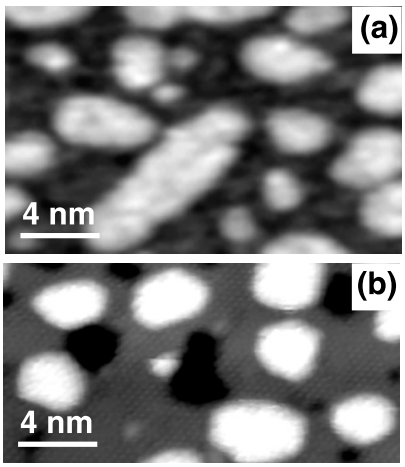

Figure 5. STM images for 0.5 ML (a) and 5 ML (b) PLD Co films deposited at 230 K and then exposed to 3000 L of CO. CO reconstruction can only be observed in 5 ML PLD Co films here.

on the bare Cu substrate. In some near edge regions of the island, a different ('delta-like')† reconstruction pattern can be observed. We assume this may be due to the CO decoration effect of a certain ordered surface alloy of Co and Cu atoms.

For PLD Co films, similar 'delta-like' local reconstructions are observed on the islands as well as on the substrate up to a Co thickness of 3 ML, cf figure 5(a). Only at higher coverage, namely from 3 ML on, can a clear $(\sqrt{3} \times \sqrt{3})R30^\circ$–CO reconstruction also be detected in the PLD Co films, figure 5(b).

In order to know how much intermixing happens in the initial stage of PLD films, we roughly estimated the intermixing measuring AES peak intensity ratio between Cu and Co because it should be different with or without intermixing. In our case, the non-overlapping peaks, i.e. the Co peak at 716 eV and the Cu peak at 920 eV, were taken into consideration.

† The term 'delta-like' is derived from our naive view of the appearance of some dominant CO reconstruction features outside the regular $(\sqrt{3} \times \sqrt{3})R30^\circ$ pattern. The use of the term 'delta' here is not related to any of the known TDP states (alpha and gamma).

Upon a closer view of the angles and interatomic distances involved in the overall reconstruction pattern of figure 4 we find that our 'delta-like' features are likely to be *remnants* of a $(\sqrt{(7/3)} \times \sqrt{(7/3)})R10.9^\circ$ superstructure desribed by Papp [20] consisting of three CO molecules forming just one unit of this reconstruction, namely one molecule in a top position and the two others in hollow positions. Papp relates this kind of reconstruction to a higher CO supersaturation at 286 K adsorption temperature. Surplus of CO we regard to be equivalent to a lack of Co in the surface in our case. From what is seen in the CITS image (figure 3(c)) there are parts of the islands different in contrast from their surroundings (e.g. the one marked '3'). Thus perhaps Cu-enriched areas could be the reason for the CO $(\sqrt{(7/3)} \times \sqrt{(7/3)})R10.9^\circ$ superstructure in parts of figure 4 consisting mainly of such 'delta-like' remnants.

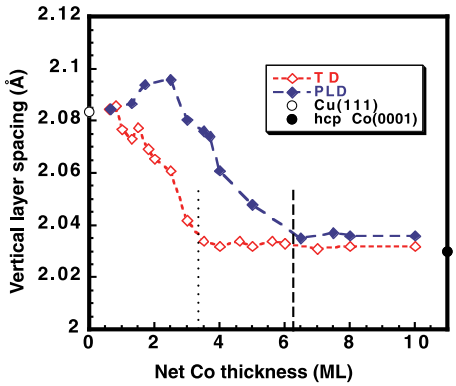

Figure 6. Calculated average interlayer distance of the PLD (full circles) and TD (open circles) Co/Cu (111) films. Also shown here are the values of the interlayer distance for bulk fcc Cu (111) and bulk hcp Co(0001). The dotted line *and* the long-dashed line indicate the position where hcp stacking becomes dominant in the films.

As an example for a 3 ML film, the experimental intensity ratio of I_{Co} at 716 eV and I_{Cu} at 920 eV is 0.599. Let us consider the theoretical ratio for two models, supposing for case (i) 5% Cu in each of the lower two layers with the top layer to be pure Co, which yields an intensity ratio I_{Co}/I_{Cu} of 0.593. For case (ii), we assume 7% Cu in the first layer, 3% Cu in the second layer with the top layer being Co, resulting in an even lesser intensity ratio I_{Co}/I_{Cu} of 0.589. From this comparison it follows that the intermixing in the PLD films does not exceed 10%.

A remarkable feature of the PLD films is the delay of the fcc→hcp structural phase transition. LEED intensity versus energy spectra (IV-LEED) are extremely sensitive to changes of the layer stacking sequences and stacking faults. Recently we have shown that hcp stacking evolves in the TD films as soon as the Co thickness exceeds 2 ML indicated by the sixfold symmetry of IV-LEED curves of (10) beams while the hcp stacking becomes noticeable in the PLD films only when the Co thickness reaches 5 ML, finally dominating the structure at higher coverages [15]. In order to obtain more quantitative data we used the (00) beam IV-LEED curves to calculate the average interlayer distance according to the kinematical model. The intensity of the (00) beam was recorded at an incident angle approximately 6° off-normal. The variation of the average interlayer distance d with the film thickness for both TD and PLD films is shown in figure 6. The dotted and the long-dashed lines indicate the critical thickness for hcp stacking becoming dominant in the TD and PLD Co films, respectively. From the d–t plot we learn that the critical thickness† for the hcp stacking is about 3 ML for TD films when the average interlayer distance of the Co films drops to the interlayer distance of bulk hcp Co(0001) $d = 2.03$ Å; while the critical thickness for PLD films is about twice the TD film value, namely 6 ML.

Accompanying the layer-by-layer growth and the delayed fcc→hcp transition, the magnetic properties for PLD films are also different from that of TD films. Figures 7 and 8 show the longitudinal and polar Kerr hysteresis loops of the TD (left column) and PLD (right column) Co/Cu(111) films, respectively. For both kinds of film, the easy magnetization axis is in plane as soon as the film thickness exceeds 2 ML. No polar easy axis Kerr loop was detected for all PLD films. For TD, on the other hand, a longitudinal Kerr loop alone was recorded

† The energy barrier for the fcc→hcp structural transformation which determines critical thickness depends on the film/substrate crystallographic orientation relation. The values for the critical thickness derived in the present paper thus are restricted to the Co/Cu(111) system.

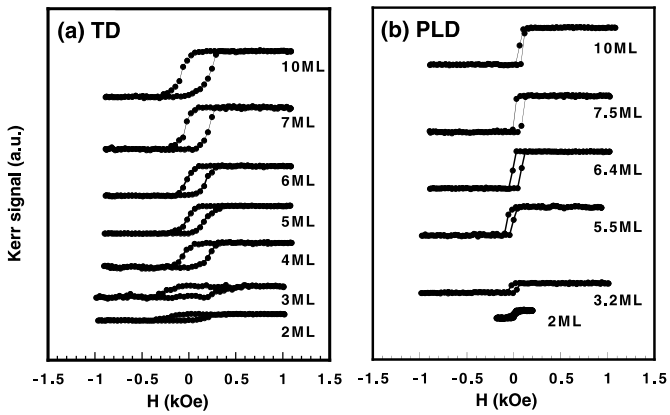

Figure 7. Longitudinal Kerr hysteresis loops for TD (left column) and PLD (right column) films measured at 230 K.

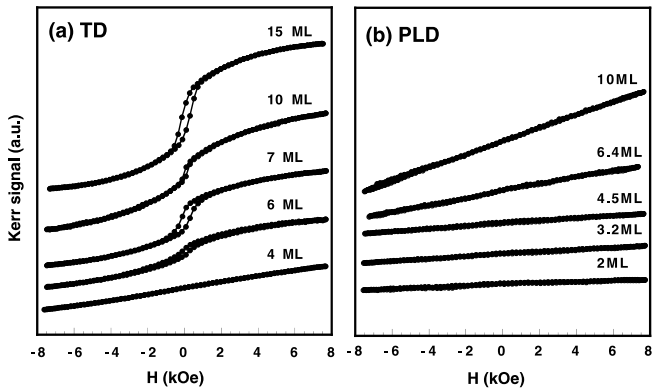

Figure 8. Polar Kerr hysteresis loops for TD (left column) and PLD (right column) films measured at 230 K. Note that for TD films polar loops start to appear when the thickness is larger than 6 ML while for PLD films no polar loop was detected for the whole range of thicknesses reached in the experiments (15 ML).

only for lower thickness films ($t_{\mathrm{Co}} < 6$ ML). Additionally a polar Kerr loop on top of the hard axis contribution of the in-plane oriented parts of the sample magnetization was observed in figure 8(a) when the Co thickness exceeds 6 ML. It should be noticed that the geometry of our MOKE allows us to clearly distinguish between polar and in-plane magnetization components because of the sample position in the centre of a homogeneous excitation field and a sample alignment within $\pm 0.5^{\circ}$ accuracy.

Improved layer-by-layer growth together with the suppression of hcp stacking faults eventually results in complete AF coupling in PLD Co/Cu/Co/Cu(111) trilayers. Figure 9 displays the polar and longitudinal MOKE loops for two Co(4 ML)/Cu(4 ML)/Co(4 ML) trilayers grown at 230 K on Cu(111) by TD and PLD respectively.

PLD was applied to the Co layers while at the same time it was tolerable to thermally evaporate (from a crucible) the Cu spacer layer in both trilayer systems. The thickness of the Cu spacer layer (4 ML) is supposed to yield maximum AF coupling [9]. The TD-grown

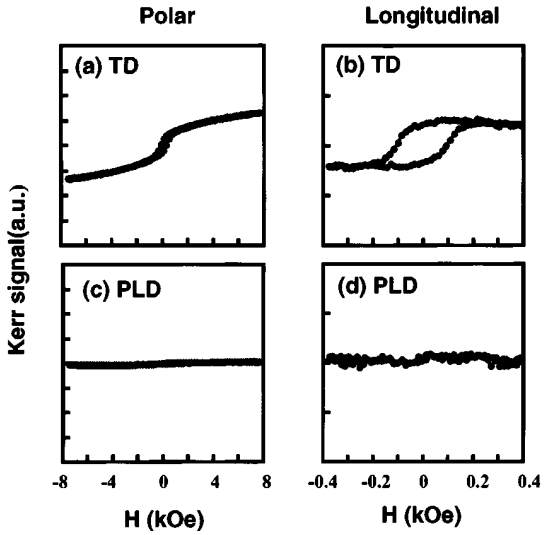

Figure 9. Polar and longitudinal Kerr hysteresis loops measured at 230 K for Co(4 ML)/Cu(4 ML)/Co(4 ML) trilayers grown on Cu(111) by TD (upper panel) and PLD (bottom panel). The cancellation of signal for both the in-plane and the out-of-plane magnetization of the PLD trilayer indicates complete antiferromagnetic coupling.

trilayer retains partial ferromagnetic coupling as demonstrated by the large remanence both in the polar and longitudinal Kerr loops. Contrary to this, the Kerr signal is close to zero in the PLD-grown trilayer for both magneto-optical configurations up to a field strength of 0.8 T which means complete AF coupling is achieved here.

4. Discussion

The difference of structural and magnetic properties in PLD and TD Co/Cu(111) films and Co/Cu/Co/Cu(111) trilayers is closely related to the growth mode of these films. The remarkable improvement in PLD growth can be attributed to the high nucleation density generated by a very high instantaneous deposition rate [16]. In PLD, the laser beam, with a duration of tens of nanoseconds, produces a plasma in front of the target by which the target atoms are set free mostly by non-thermal bond breaking processes. The deposition occurs within 0.5 to 1 μs after each pulse, depending on the distance from the target to the substrate. Subsequently, a long pause follows, of the order of 10^5 μs given by the repetition rate of 5 Hz used in our experiment. The laser energy is set just slightly above the threshold energy for this non-thermal process to avoid droplet formation and deposition. The liberated atoms, predominantly neutrals, have a rather wide energy distribution with a peak around 1 eV although the tail of the energy distribution, made up of ionized atoms, may reach up to several 10 eV but with low intensity. Under these conditions, the deposition rate is 0.001 to 0.0005 ML per laser shot, resulting in an extremely high *instantaneous* deposition rate of about 10^3 ML s^{-1} whereas the *average* rate amounts to about 0.2 ML min^{-1} at the chosen repetition frequency of 5 Hz. The instantaneous rate in the range of 10^3 ML s^{-1}, which is more than five orders of magnitude higher than in thermal deposition under usual MBE conditions, leads to a considerably higher flux F of material than in conventional methods. Following the scaling relationship, the island density N during nucleation and growth can be given by $N \sim (F/D)^{\gamma}$

[19], with D the surface diffusion rate and γ a parameter (with $0 < \gamma < 1$) which accounts for the size of the critical nucleus. Both increasing F and decreasing D lead to an increase in the density of nuclei. In PLD carried out under conditions set in our experiments the flux F is larger by five to six orders of magnitude compared to TD. Further a lower diffusion rate is achieved by lowering the deposition temperature. At reduced temperature—in our case for both the PLD and the TD experiments—and higher rates (this holds only for PLD), the arriving atoms do not have enough time to find the nearest nucleation centre and nucleate spontaneously into small islands [21]. Thus, a high nucleation density is obtained as shown by many features of monatomic height as small as only a few nm in our STM images of PLD films. Adatoms occasionally landing on their top can therefore reach the edge of the island much more frequently and thus have a higher probability to overcome the step edge barrier and subsequently fill the lower layer *before* they meet other diffusing species on top of the island to form the next higher level. The existing islands of the just growing level thus grow by incorporating atoms that arrive nearby or fall down from the top and eventually merge into a completely filled monolayer.

In our previous paper [15], we addressed the delay of the fcc→hcp transition as the result of improved layer-by-layer growth. We assume there is a certain critical thickness above which the Co films start to transform from fcc into hcp structure since the natural hcp phase of Co at room temperature is more energetically favourable. Due to the 3D island growth, the thickness of the islands of the TD films already exceeds the critical thickness locally despite the nominal thickness being lower. So hcp structure already becomes dominant in the TD films when the *nominal* Co thickness is larger than 3 ML while the PLD films reach the critical thickness just at 6 ML because of layer-by-layer growth. Thus, the local thickness of the fcc→hcp structural transition in the Co/Cu(111) epitaxial system can be deduced to be around 6 ML.

The surface orientation is an 'intrinsic' parameter which influences the thickness for the fcc to hcp phase transformation. In contrast to the Cu(110) surface† on the Cu(111) surface the Co fcc to hcp transition requires only a slip in the (0001) Co basal plane or the incorporation of a stacking fault in the fcc structure during growth which might be the main reason why only very few monolayers of fcc Co can be grown on Cu(111).

In this context we want to mention that of the Cu(111) orientation is important because this is—together with (100)—the favoured texture during growth on technologically relevant polycrystalline and amorphous substrates.

It is not surprising then that the TD films show additional polar Kerr hysteresis loops when their nominal thickness exceeds 6 ML since the 3D islands of the TD films possibly locally reach the thickness (>10 ML) to exhibit bulk hcp Co magnetic properties with easy axis out of plane. Due to the still dominant shape anisotropy, it is impossible for the TD Co films to have complete out-of-plane magnetic anisotropy, while for the PLD films the layer-by-layer growth lasts up to 8 ML and does not deviate too much from this growth mode even at 15 ML. So the PLD films exhibit in-plane anisotropy at all thicknesses we reached in our experiment.

A direct consequence of the improved 2D growth and of the suppression of hcp stacking faults is the complete AF coupling achieved in Co(4 ML)/Cu(4 ML)/Co(4 ML)/Cu(111) trilayers by depositing alternately Co (by PLD) and Cu (by TD). This method eliminates the twinning structure in the Cu spacer layer and thus diminishes the density of trenches or pinholes in the spacer layer substantially leading to complete AF coupling for both in-plane and out-of-plane magnetization [15, 22].

In summary, we have found that layer-by-layer growth in Co/Cu(111) films can be achieved by pulsed laser deposition. Although interdiffusion between Co and Cu atoms happens in

† Where it is possible to stabilize fcc Co at least up to 15 monolayers [12].

the early stage, the interdiffusion is less than 10% in the first two monolayers and does not go beyond these two layers. The improved layer-by-layer growth is attributed to the high nucleation density caused by a high instantaneous deposition rate. With layer-by-layer growth, there is a delay of the fcc to hcp phase transition in the PLD Co films compared to the TD Co films. The magnetic behaviour of the PLD films is also different from that of the TD films where a hysteresis loop in the perpendicular direction is detected as soon as the hcp structure is dominant in the TD films. In addition, a complete antiferromagnetic coupling in Co/Cu/Co/Cu(111) trilayers by PLD is achieved for both in-plane and out-of-plane magnetization directions.

Acknowledgments

The authors would like to thank G Kroder for his technical support.

References

[1] Parkin S S P, Bahdra R and Roche K P 1991 *Phys. Rev. Lett.* **66** 2152
[2] Egelhoff W F Jr and Kief M T 1992 *Phys. Rev.* B **45** 7795
[3] Johnson M T, Coehoorn R, de Vries J J, McGee N M W, ann de Stegge J and Bloemen P H 1992 *Phys. Rev. Lett.* **69** 969
[4] Parkin S S P, Marks R F, Farrow R F C, Harp G R, Lam Q H and Savoy R J 1992 *Phys. Rev.* B **46** 9262
[5] Kohlhepp J, Elmers H J and Gradmann U 1993 *J. Magn. Magn. Mater.* **121** 487
[6] de la Figuera J, Prieto J E, Ocal C and Miranda R 1993 *Phys. Rev.* B **47** 13 043
[7] Pedersen M Ø, Bønicke I A, Laegsgaard E, Stensgaard I, Ruban A, Nørskov J K and Besenbacher F 1997 *Surf. Sci.* **387** 86
[8] Camarero J, Spendeler L, Schmidt G, Heinz K, de Miguel J J and Miranda R 1994 *Phys. Rev. Lett.* **73** 2448
[9] Camarero J, Graf T, de Miguel J J, Miranda R, Kuch W, Zharnikov M, Dittschar A, Schneider C M and Kirschner J 1996 *Phys. Rev. Lett.* **76** 4428
[10] Tonner B P, Han Z-L and Zhang J 1993 *Phys. Rev.* B **47** 9723
[11] Rath C, Prieto J E, Müller S, Miranda R and Heinz K 1997 *Phys. Rev.* B **55** 10 971
[12] Toelkes C, David R, Tschersich K G, Comsa G and Zeppenfeld P 1999 *Europhys. Lett.* **46** 589
[13] Kuch W, Dittschar A, Lin M-T, Salvietti M, Zharnikov M, Schneider C M, Kirschner J, Camarero J, de Miguel J J and Miranda R 1997 *J. Magn. Magn. Mater.* **170** L13
[14] Shen J, Ohresser P, Mohan C V, Klaua M, Barthel J and Kirschner J 1998 *Phys. Rev. Lett.* **80** 1980
Jenniches H, Klaua M, Höche H and Kirschner J 1996 *Appl. Phys. Lett.* **69** 3339
[15] Zheng M, Shen J, Mohan C V, Ohresser P, Barthel J and Kirschner J 1999 *Appl. Phys. Lett.* **74** 425
[16] Ohresser P, Shen J, Barthel J, Zheng M, Mohan C V, Klaua M and Kirschner J 1999 *Phys. Rev.* B **59** 3696
[17] Hamers R J, Tromp R M and Demuth J E 1986 *Phys. Rev. Lett.* **56** 1972
[18] Kirstein W, Kruger B and Thieme F 1986 *Surf. Sci.* **176** 505
[19] Bridge M E, Comrie C M and Lambert R M 1977 *Surf. Sci.* **67** 393
[20] Papp H 1983 *Surf. Sci.* **129** 205
[21] Himpsel F J, Ortega J E, Mankey G J and Willis R F 1998 *Adv. Phys.* **47** 511
[22] Zheng M, Shen J, Barthel J, Mohan C V, Ohresser P and Kirschner J 1998 unpublished